Disorder effects in alloy superlattices

D. Z.-Y. Ting and Yia-Chung Chang
Department of Physics and Materials Research Laboratory, University of Illinois at Urbana-Champaign, Urbana, Illinois 61801
(Received 20 July 1987; revised manuscript received 22 December 1987)

We examine the effects of disorder on superlattices made of semiconductor alloys by proposing a method for obtaining an approximate solution of the coherent-potential approximation for superlattices. Our method is tested on a model one-dimensional superlattice for which it is possible to generate the "exact" densities of states with a Monte Carlo method. Our results are shown to be in good agreement with the Monte Carlo results. As an example of how this method might be implemented for realistic systems, we have computed the density of states and self-energies for $Al_xGa_{1-x}As/Al_yGa_{1-y}As$ superlattices.

I. INTRODUCTION

Semiconductor alloys are frequently used in the growth of semiconductor superlattices. The use of the alloys are important because they offer a simple way to tailor the superlattice electronic and optical properties. In the $GaAs/Al_xGa_{1-x}As$ superlattice, for instance, one could adjust the barrier heights of the quantum wells by varying the composition of the $Al_xGa_{1-x}As$ alloy. Since substitutional disorder is always present in these semiconductor alloys, it is of scientific as well as practical interest to investigate the effects of disorder on the electronic properties of superlattices. One method for studying the effect of disorder is the coherent-potential approximation[1-3] (CPA) which, within the framework of the single-site approximation (SSA),[2] is considered to be the best among the existing theories for treating disorder. Previously, the CPA has been used extensively to study the effects of disorder on the electronic and optical properties of bulk semiconductors.[4-7] Because of the two-dimensional nature of the confined states in superlattices, the effect of disorder is expected to be more pronounced than in bulk, three-dimensional (3D) alloy semiconductors. However, due to the large amount of computation required, there have been no attempt to perform CPA calculations for realistic superlattices.[8]

In this paper we propose a method for efficiently obtaining an approximate solution to the CPA equations for superlattices. The approximation scheme is tested on a 1D linear-chain model for which it is possible to efficiently generate the "exact" densities of states using a Monte Carlo method. We also present some results on $Al_xGa_{1-x}As/Al_yGa_{1-y}As$ superlattices to demonstrate how our method might be applied to realistic superlattices.

II. THEORY

Consider superlattices made from the alloys of materials C and D. We use the notation $(L_W,L_B)\ C_xD_{1-x}/C_yD_{1-y}$ to describe a superlattice in which each period consists of L_W layers of well material C_xD_{1-x}, followed by L_B layers of barrier material C_yD_{1-y}. (It should be noted that our theoretical treatment is still applicable if the barrier material is an alloy made of materials other than C and D.) The typical approach taken in treating such a system is to invoke the virtual-crystal approximation (VCA) and consider the alloys in the superlattices as fictitious materials whose properties are determined by weighted averages of the materials C and D. The VCA Hamiltonian is given by

$$H_0=\begin{cases} xH^C+(1-x)H^D & \text{in the well region}, \\ yH^C+(1-y)H^D & \text{in the barrier region}, \end{cases} \tag{1}$$

where H^C and H^D are the Hamiltonians for the pure bulk materials C and D. The VCA Hamiltonian is periodic with the periodicities of the superlattice, and can be treated by known solid-state techniques. Although the VCA completely ignores the effects of disorder, it serves as a good starting point for treating the alloy problem.

To include the disorder effects, we write the full Hamiltonian as

$$H=H_0+V\ , \tag{2}$$

where V is the disorder potential. Following the usual procedure,[3] we define the self-energy operator $\Sigma(E)$ in conjunction with the configuration-averaged single-particle Green's function:

$$\langle G(E)\rangle=\left\langle\frac{1}{E-H_0-V}\right\rangle\equiv\frac{1}{E-H_0-\Sigma(E)}\ , \tag{3}$$

where the angular brackets $\langle\ \rangle$ are used to denote the average taken over all possible configurations of the C_xD_{1-x}/C_yD_{1-y} superlattice. $\Sigma(E)$ is complex, and energy dependent, and may be viewed as an effective potential which represents the effect of the disorder potential V. Knowing $\langle G(E)\rangle$, or equivalently, $\Sigma(E)$, allows us to compute properties such as density of states and optical absorption. To determine $\Sigma(E)$ we invoke the well-known single-site approximation (SSA).[2,3] We define a reference potential $\bar{V}(E)$. Assume that V, $\bar{V}(E)$, and $\Sigma(E)$ can be decomposed into a sum of contributions from individual unit cells:

$$V=\sum_n v_n \mid n\rangle\langle n \mid \ , \tag{4}$$

$$\tilde{V}=\sum_n \tilde{v}_n \mid n\rangle\langle n \mid \ , \tag{5}$$

$$\Sigma=\sum_n \sigma_n \mid n\rangle\langle n \mid \ , \tag{6}$$

where $\mid n\rangle$ is a basis orbital located at the unit cell labeled n. It can be shown that within the single-site approximation σ_n is given by[2,3]

$$\sigma_n=\tilde{v}_n+\langle t_n\rangle(1+\tilde{G}_n\langle t_n\rangle)^{-1} \ , \tag{7}$$

where

$$\tilde{G}_n\equiv\langle n \mid \tilde{G} \mid n\rangle\equiv\langle n \mid [E-H-\tilde{V}(E)]^{-1} \mid n\rangle \ ,$$

and $\langle t_n\rangle$ is the averaged t matrix representing the averaged scattering relative to the reference medium $\tilde{V}(E)$ due to a single scatterer v_n at site n:

$$\langle t_n\rangle=\langle (v_n-\tilde{v}_n)[1-\tilde{G}_n(v_n-\tilde{v}_n)]^{-1}\rangle \ . \tag{8}$$

Note that for the sake of clarity we have assumed that only one basis orbital per unit cell ($\mid n\rangle$) is used, and treated $\sigma_n, t_n, \ldots$, etc. as scalars. In general, there are more than one orbital per unit cell, and the SSA equations are matrix equations.

Equations (7) and (8) are known as the SSA equations, and they serve as the starting point of our treatment of alloy superlattices. Although the SSA equations were originally developed to treat bulk alloys, they are perfectly applicable to alloy superlattices. The only difference is this: In the case of the bulk alloy, v_n is the same random variable for all sites n, and σ_n is site independent. Therefore, we only need to solve the SSA equations for any single site. In the case of the superlattice, however, the set of random variables $\{v_n\}$ are not identical for all sites, and there are $L=L_W+L_B$ distinct σ_n's to be solved for, one each for the L inequivalent layers in the superlattice. Note that the SSA equations for different sites are coupled through $\tilde{G}$, which depends on the value of $\tilde{V}$ at all sites.

To self-consistently solve the SSA equations for alloy superlattices, we use a technique due to Chen[9] called the iterated average-t-matrix approximation (IATA).

With the IATA we can converge on the CPA solutions quickly by calculating σ_n iteratively. The technique was developed for solving the SSA equations for bulk alloys, but can be extended to treat alloy superlattices in a straightforward manner. The procedure is as follows: We start out with a set of initial guesses to the correct $\{\sigma_n\}$, namely, $\{\tilde{v}_n\}$. Use $\{\tilde{v}_n\}$ as the input for Eq. (8) and compute the set of single-site averaged t matrices $\{\langle t_n\rangle\}$. If the $\langle t_n\rangle$'s are zero (or, in practice, smaller than a predefined tolerance), then we say that the CPA condition is met, and that $\{\tilde{v}_n\}$ is the desired $\{\sigma_n\}$ by virtual of Eq. (7). If the CPA condition is not met, we use the set of $\{\langle t_n\rangle\}$ as input for Eq. (7) and obtain a set of $\{\sigma_n\}$. We then use the $\{\sigma_n\}$ as the new set of guesses $\{\tilde{v}_n\}$, and repeat the procedure until the CPA condition is finally met.

In evaluating the SSA equations, the most difficult quantity to compute is $\tilde{G}_n$, which, with the aid of Dyson's equation, can be written as

$$\langle n \mid \tilde{G}(E) \mid n\rangle=\langle n \mid [1-G_0(E)\tilde{V}(E)]^{-1}G_0(E) \mid n\rangle \ , \tag{9}$$

where $G_0(E)\equiv(E-H_0)^{-1}$ is the unperturbed Green's function. To properly evaluate $\tilde{G}_n(E)$ involves (1) transforming the problem into the superlattice basis where G_0 is block diagonal in $L\times L$ blocks, (2) computing the matrix element of $G_0(E)$, each of which is an E-dependent one-dimensional integral, and (3) inverting an $L\times L$ matrix $[1-G_0(E)\tilde{V}(E)]^{-1}$ for each E. In addition, remember that this process must be repeated for each iteration in the IATA procedure. As we can see, this is quite impractical due to the amount of computation involved.

To circumvent this problem we make the following approximation: We note that $\tilde{V}$ is a smoothly varying function of position. In evaluating $\tilde{G}$ in the SSA equations at site l, we approximate $\tilde{V}$ by its value at site l and write

$$\begin{aligned}\tilde{V}(E)&\approx\sum_n \tilde{v}_l(E) \mid n\rangle\langle n \mid \\ &=\tilde{v}_l(E)\sum_n \mid n\rangle\langle n \mid \ .\end{aligned} \tag{10}$$

This, in turn, allows us to write

$$\tilde{G}_l(E)\approx\left\langle l\left|\frac{1}{E-H_0-\tilde{v}_l}\right|l\right\rangle \ . \tag{11}$$

Note that by making this approximation we have decoupled the l site from the other sites. Note also that this approximation becomes exact in the bulk alloy case.

With the above approximation we can evaluate $\tilde{G}_l(E)$ as follows:

$$\begin{aligned}\tilde{G}_l(E)&\approx\left\langle l\left|\frac{1}{E-H_0-\tilde{v}_l}\right|l\right\rangle \\ &=\sum_\nu \frac{\langle l \mid \nu\rangle\langle \nu \mid l\rangle}{E-\tilde{v}_l-E_\nu} \\ &=\int dE'\frac{1}{E-\tilde{v}_l-E'}\sum_\nu \langle l \mid \nu\rangle\langle \nu \mid l\rangle\delta(E'-E_\nu) \\ &\equiv\int dE'\frac{\rho_l^0(E')}{E-\tilde{v}_l-E'} \ .\end{aligned} \tag{12}$$

In the equation above E_ν and $\mid \nu\rangle$ are, respectively, the νth eigenvalue and eigenstate of the VCA superlattice Hamiltonian. $\rho_l^0(E)$ is the local density of states associated with the site l.

The CPA density of states for superlattices can be obtained by calculating the imaginary part of the trace of the CPA Green's function over the VCA eigenstates $\mid \nu\rangle$:

$$\rho(E)=-\frac{1}{\pi N}\mathrm{Im}\,\mathrm{Tr}G^{\mathrm{CPA}}(E)$$
$$=-\frac{1}{\pi N}\mathrm{Im}\sum_{\nu}\langle\nu\,|\,G^{\mathrm{CPA}}(E)\,|\,\nu\rangle\ , \tag{13}$$

where

$$G^{\mathrm{CPA}}(E)\equiv[E-H_0-\Sigma(E)]^{-1}\ . \tag{14}$$

By multiplying both sides of Eq. (14) by $[E-H_0-\Sigma(E)]$, it can be shown that

$$\delta_{\mu\nu}=(E-E_\mu)g_{\mu\nu}-\sum_{\eta}\sigma_{\mu\eta}g_{\eta\nu}\ , \tag{15}$$

where $g_{\mu\nu}(E)\equiv\langle\mu\,|\,G^{\mathrm{CPA}}(E)\,|\,\nu\rangle$ and $\sigma_{\mu\nu}(E)\equiv\langle\mu\,|\,\Sigma(E)\,|\,\nu\rangle$.

Now note that as the disorder potential $V\to 0$, $g_{\mu\nu}\to\delta_{\mu\nu}g_{\nu\nu}$. For V reasonably small, we expect the dominant contribution to the sum in the above equation to come from the term containing $g_{\nu\nu}$. We can therefore approximate the sum by this dominant term and write

$$\delta_{\mu\nu}\approx(E-E_\mu)g_{\mu\nu}-\sigma_{\mu\nu}g_{\nu\nu}\ . \tag{16}$$

For $\mu=\nu$, we could solve for $g_{\nu\nu}$ directly and obtain

$$g_{\nu\nu}(E)=\frac{1}{E-E_\nu-\sigma_{\nu\nu}}\ . \tag{17}$$

It can be easily shown that $\sigma_{\nu\nu}(E)$ is given by

$$\sigma_{\nu\nu}(E)=\sum_{n}|\,C_n^\nu\,|^2\sigma_n(E)\ , \tag{18}$$

where the coefficients C_n^ν's are the components of the νth eigenvector:

$$|\,\nu\rangle=\sum_{n}C_n^\nu\,|\,n\,\rangle\ . \tag{19}$$

Note that this has a simple interpretation. Equation (18) says that $\sigma_{\nu\nu}$, the coherent potential associated with the state $|\,\nu\rangle$, is an average of the σ_n's belonging to the different sites, weighted according to the charge density associated with $|\,\nu\rangle$.

III. RESULTS AND DISCUSSION

In this section we apply our approximation to two examples. In Sec. III A we examine a one-dimensional linear-chain model as a test case, and in Sec. III B we examine some $Al_xGa_{1-x}As/Al_yGa_{1-y}As$ superlattices.

A. One-dimensional superlattice

In the theory section we have not rigorously justified our approximation. Here we try to see how well this approximation works by testing it on a 1D linear-chain model for which it is possible to obtain the exact density of states for comparison. We examine a simple 1D (L_W,L_B) C_xD_{1-x}/C_yD_{1-y} superlattice for which we only include on-site energies and nearest-neighbor interactions. The nearest-neighbor interaction is taken to be the same in the entire chain (i.e., no off-diagonal disorder), while the on-site energy is treated as a random variable. The Hamiltonian for this system can be written as

$$H=\sum_{n=1}^{N}[E_n\,|\,n\rangle\langle n\,|$$
$$+T(\,|\,n-1\rangle\langle n\,|+|\,n+1\rangle\langle n\,|\,)]\ , \tag{20}$$

where N is the number of atoms in the chain, T is the nearest-neighbor interaction, and E_n is the on-site energy at site n. E_n can take on the value of E_C or E_D, depending on whether the atom at site n is C or D. The density of states of this superlattice can be computed numerically using a very efficient method due to Dean.[10] The method has previously been used extensively to calculate phonon[11] and electron[12] densities of states for disordered linear chains. It allows us to obtained the density of states without explicitly knowing the eigenvalues, i.e., without performing matrix diagonalization. We could therefore very efficiently perform Monte Carlo calculations on a large random linear-chain superlattice and obtain the "exact" density of states for comparison with our results.

As an example, we consider the random linear-chain superlattice (10,10) $C_{0.8}D_{0.2}/D$ (i.e., $L_W=10$, $L_B=10$, and $x=0.8$, $y=0$). The on-site energies are taken to be $E_C=3.0$ eV and $E_D=3.5$ eV, and the nearest-neighbor

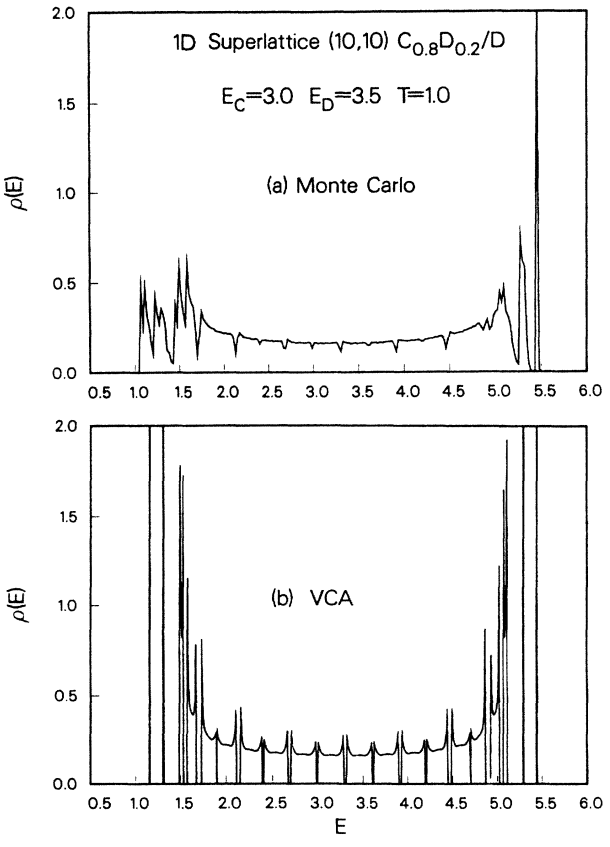

FIG. 1. Density of states for the random linear-chain superlattice (10,10) $C_{0.8}D_{0.2}/D$ as obtained by the Monte Carlo method and by the virtual-crystal approximation.

interaction is $T=1$ eV. Figures 1(a) and 1(b) show the density of states for this linear-chain superlattice as obtained, respectively, by the Monte Carlo method, and by the virtual-crystal approximation (VCA). We see that while the VCA does an adequate job in predicting the overall shape of the true (Monte Carlo) density of states, there are some important differences. The VCA spectrum is separated by 19 minigaps into 20 segments (corresponding to the 20 subbands for this superlattice). In the Monte Carlo spectrum the minigaps have disappeared due to disorder broadening. Note that the VCA does a much better job at the upper end of the spectrum than at the lower end. This is mainly due to the composition of this particular superlattice. The upper end of the spectrum corresponds to the unconfined states which are primarily localized in the barrier region (the so-called antiwell states). Since for this example there is no disorder in the barrier region, the VCA results are quite satisfactory. The lower end of the spectrum, on the other hand, are made up of the confined states which are primarily in the well ($C_{0.8}D_{0.2}$ alloy) region where the effects of disorder must be taken into account. Since the VCA ignores the disorder effects, it fails to give a good description of the densities associated with the confined states.

In Fig. 2 we take a closer look at the confined states by examining the density of states from 1.0 to 1.5 eV. The VCA confined-state spectrum (dotted curve) shows two narrow peaks corresponding to the two lowest subbands. The Monte Carlo spectrum (histogram) is considerably richer in features, showing substantial disorder broadening. Note that the broadening is highly asymmetrical about the positions of VCA peaks. The CPA spectrum (dashed curve) compares very favorably with the Monte Carlo results. (Note: by "CPA" we mean our approximate solution to the CPA; the same applies to all the labels in our figures.) In particular, the CPA correctly predicts the closing of the minigaps as well as the asymmetric broadening of the confined-state peaks. Note that the Monte Carlo result contains some fine structures not found in the CPA spectrum. The smoothness of our CPA spectrum is characteristic of the single-site CPA theories (recall that with our approximation the sites are decoupled).

We should point out that by performing calculations similar to the above, we find that our approximation tends to underestimate the effects of disorder on the bound quantum-well states for superlattices in which only the barrier layers are disordered. This is probably because of the fact that we have decoupled the sites, and the disorder in the barrier region is not "communicated" well enough to the bound states which are primarily located in the well region.

B. $Al_xGa_{1-x}As/Al_yGa_{1-y}As$ superlattices

In this section we apply our superlattice CPA theory to some $Al_xGa_{1-x}As/Al_yGa_{1-y}As$ superlattices. We concentrate our effort on studying how the confined states are affected by disorder. In these calculations we start out with the VCA, and then treat the remaining disorder potential with CPA. In our CPA treatment we have used the method of Chen and Sher[5] of casting the disorder potential in the bond-orbital model[13] basis in which the off-diagonal disorder is much smaller than the diagonal disorder. This allows us to ignore the off-diagonal disorder to the first approximation. In addition, structural disorder[14–16] is also disregarded in this calculation. The VCA electronic structures of the $Al_xGa_{1-x}As$ superlattices are calculated by the one-band Wannier orbital model as described in Ref. 17.

We first consider a (20,20) $Al_{0.2}Ga_{0.8}As/Al_{0.6}Ga_{0.4}As$ superlattice. Figure 3 shows the conduction-band density of states for this superlattice as computed by the VCA and CPA. The energy range is in the confined-state region. In our calculation the disorder experienced by the conduction-band states arises from the difference between

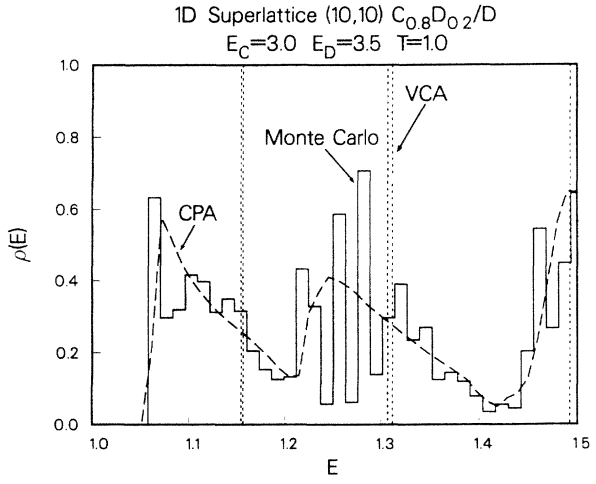

FIG. 2. Density of states for the random linear-chain superlattice (10,10) $C_{0.8}D_{0.2}/D$ in the confined-state energy range as obtained by the Monte Carlo method (histogram), VCA (dotted curve), and CPA (dashed curve).

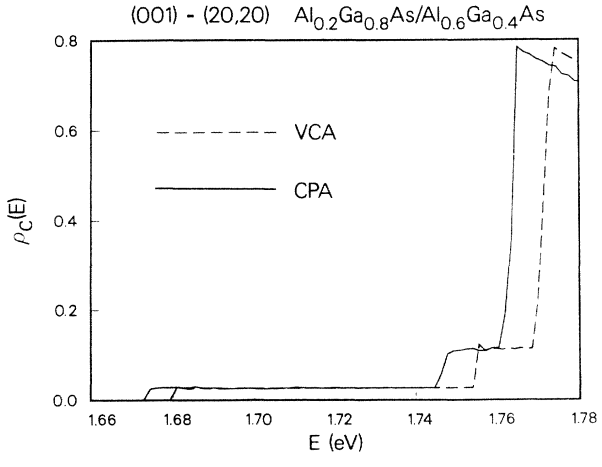

FIG. 3. Conduction-band density of states for the (20,20) $Al_{0.2}Ga_{0.8}As/Al_{0.6}Ga_{0.4}As$ superlattice in the confined-state energy range as obtained by VCA (dashed curves) and CPA (solid curves).

the antibonding energies (ε_a) of AlAs and GaAs. For this example we have used $\varepsilon_a(\text{AlAs})=6.114$ eV and $\varepsilon_a(\text{GaAs})=6.310$ eV. The numbers are taken from Chen and Sher,[5] but adjusted to conform with the recently reported band-offset value of $Q_e=0.7$ (Refs. 18–20) (meaning that 70% of the direct-band-gap difference between the well and barrier materials is associated with the conduction band). This gives us a rather small scattering strength of $\delta_a=\varepsilon_a(\text{GaAs})-\varepsilon_a(\text{AlAs})=0.196$ eV. However, as we can see from Fig. 3 by comparing the VCA and CPA results, the effects of disorder on the superlattice density of states is quite visible. Most noticeably, we see that the CPA spectrum is down-shifted ~ 10 meV from the VCA spectrum.

Next, we consider a (7,14) $Al_{0.3}Ga_{0.7}As/Al_{0.7}Ga_{0.3}As$ superlattice. This differs from the previous example in that whereas the lowest confined state in the (20,20) $Al_{0.2}Ga_{0.8}As/Al_{0.6}Ga_{0.4}As$ superlattice is made up of electrons from the Γ valley, the lowest confined states in the (7,14) $Al_{0.3}Ga_{0.7}As/Al_{0.7}Ga_{0.3}As$ superlattice is made up of electrons from the X and L valleys. As before, we examine the conduction-band density of states for this superlattice in the confined-state energy range (see Fig. 4). We note that again the CPA spectrum is down-shifted ~ 8 meV from the VCA spectrum. In addition, some of the sharp peaks in the VCA spectrum are broadened.

The density of states shown in this figure actually consists of contributions from different regions of the Brillouin zone. Namely, from regions around $\mathbf{k}_\parallel=(0,0)$, $\mathbf{k}_\parallel=(1,0)$, and $\mathbf{k}_\parallel=(0.5,0.5)$ (in units of $2\pi/a$). In Fig. 5(a) we plot these three contributions separately. We note that rather than the steplike density of states which we normally expect for superlattices, there are some sharp peaks present in the VCA spectrum associated with the $\mathbf{k}_\parallel\approx(1,0)$ and $\mathbf{k}_\parallel\approx(0.5,0.5)$ regions. These peaks are the results of the anisotropies present in the superlattice band structure. The details of the origins of the anisotropy are discussed elsewhere.[17] However, it is relevant to point out here that the states near $\mathbf{k}_\parallel=(0,0)$ and $\mathbf{k}_\parallel=(1,0)$ are derived from the bulk X-valley states, and their densities are concentrated mainly in the barrier region (the X-point energy of $Al_{0.7}Ga_{0.3}As$, the barrier material, is lower than that of $Al_{0.3}Ga_{0.7}As$, the well material). The states near $\mathbf{k}_\parallel=(0.5,0.5)$ are derived from the bulk L-valley states, and their densities are concentrated mainly in the well region.

In Fig. 5(b) we expand the vertical scale of Fig. 5(a) and examine the "tails" in the CPA density of states. Note that while the VCA spectrum for the $\mathbf{k}_\parallel\approx(0.5,0.5)$ states is cut off at ~ 1.845 eV, the corresponding CPA spectrum tails all the way down to ~ 1.733 eV. A similar tail is also found for the CPA spectrum for the $\mathbf{k}_\parallel\approx(1,0)$ states. The presence of these tails indicates disorder-induced intervalley scattering in this superlattice.

Figure 6(a) and 6(b), respectively, shows the real and imaginary parts of the coherent potential $\sigma_\lambda(E)$ for the (7,14) $Al_{0.3}Ga_{0.7}As/Al_{0.7}Ga_{0.3}As$ superlattice. The individual graphs in these two figures are labeled by their layer numbers (λ), and their baselines are indicated by the

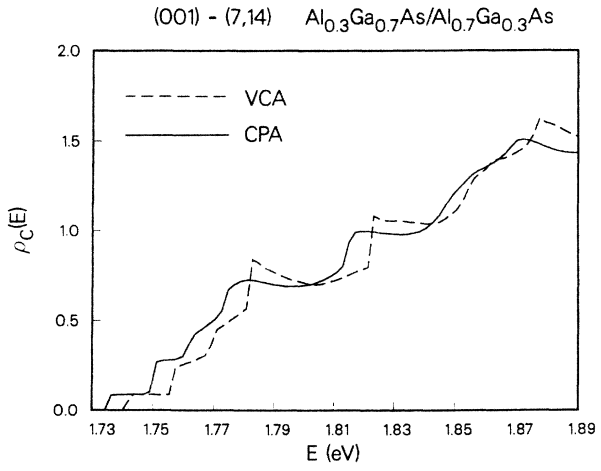

FIG. 4. Conduction-band density of states for the (7,14) $Al_{0.3}Ga_{0.7}As/Al_{0.7}Ga_{0.3}As$ superlattice in the confined-state energy range as obtained by VCA (dashed curves) and CPA (solid curves).

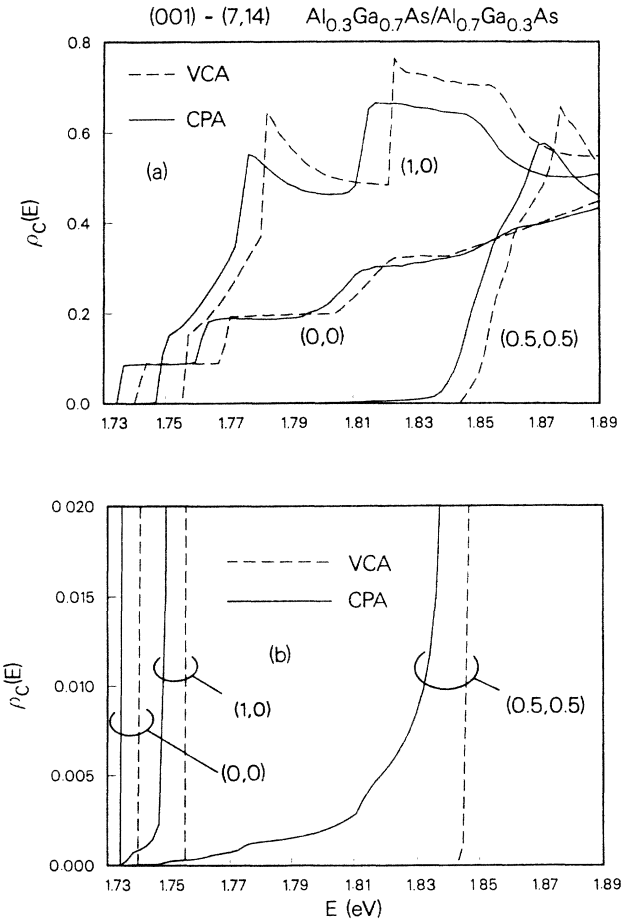

FIG. 5. Contributions to the (7,14) $Al_{0.3}Ga_{0.7}As/Al_{0.7}Ga_{0.3}As$ superlattice conduction-band density of states from different regions of the Brillouin zone.

dashed lines. For $\mathrm{Re}\sigma_\lambda(E)$, the baselines are at -0.0103 eV, and the distance between successive baselines is 0.004 eV. For $\mathrm{Im}\sigma_\lambda(E)$, the baselines are at 0 eV, and the distance between successive baselines is 0.0025 eV. For this

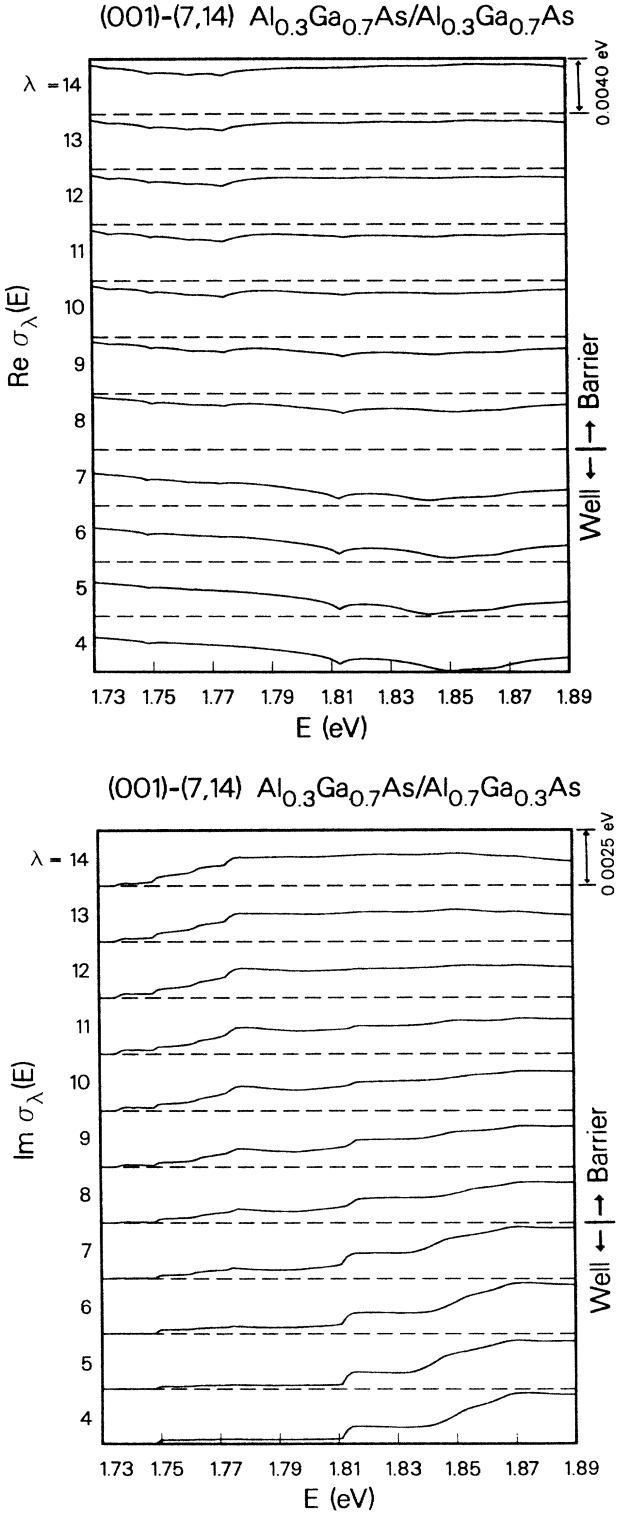

FIG. 6. (a) The real part of the coherent potential $\sigma_\lambda(E)$ for the (7,14) $Al_{0.3}Ga_{0.7}As/Al_{0.7}Ga_{0.3}As$ superlattice. (b) The imaginary part of the coherent potential $\sigma_\lambda(E)$ for the (7,14) $Al_{0.3}Ga_{0.7}As/Al_{0.7}Ga_{0.3}As$ superlattice.

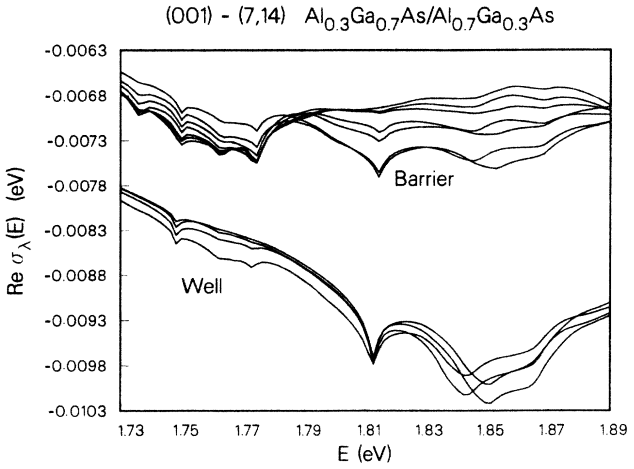

FIG. 7. The real part of the coherent potential $\sigma_\lambda(E)$ for the (7,14) $Al_{0.3}Ga_{0.7}As/Al_{0.7}Ga_{0.3}As$ superlattice.

particular superlattice, $\lambda=1,2,\ldots,7$ correspond to the well ($Al_{0.3}Ga_{0.7}As$) region, and $\lambda=8,9,\ldots,21$ correspond to the barrier ($Al_{0.7}Ga_{0.3}As$) region. Since there is symmetry about the centers of the wells and barriers, we only plot $\sigma_\lambda(E)$ for $\lambda=4,5,\ldots,14$. Note that the well center is located at $\lambda=4$, and the barrier center is between $\lambda=14$ and 15.

The amount that the energy level of a VCA state with energy E is shifted due to disorder is determined by a weighted average of all the $\mathrm{Re}\sigma_\lambda(E)$'s. In Fig. 6(a), we see that in the energy range that we are investigating, all the $\mathrm{Re}\sigma_\lambda(E)$'s are negative. The down shifting of the CPA spectrum from the VCA spectrum that we observed in Fig. 4 is a direct consequence of this. Note that if we plot all of the $\mathrm{Re}\sigma_\lambda(E)$'s together (see Fig. 7), we find that they separate into two distinct groups, namely, those that are associated with the well region, and those with the barrier region. This stems from the fact that the disorder potential in the well region and disorder potential in the barrier region are two distinct random variables.

The $\mathrm{Im}\sigma_\lambda(E)$'s give us information about how the VCA states are broadened by the disorder potential. They are complicated functions of energy as well as the layer number λ. At $E=1.75$ eV, for instance, the maximum of $\mathrm{Im}\sigma_\lambda$ occurs at the barrier center, and decreases as we go towards the well center. The opposite is true for $E=1.87$ eV. This is because the magnitude of $\mathrm{Im}\sigma_\lambda(E)$ depends on the amount of electron density with energy E present at layer λ. At $E=1.75$ eV, the electrons are in the $\mathbf{k}_\parallel\approx(0,0)$ and $\mathbf{k}_\parallel\approx(1,0)$ confined states, which, as we discussed before, are concentrated in the barrier region. At $E=1.87$ eV, we have a peak in the density associated with the $\mathbf{k}_\parallel\approx(0.5,0.5)$ confined states, which are concentrated in the well region.

IV. SUMMARY

We have developed a method for obtaining an approximate solution to the CPA scheme for superlattices made from semiconductor alloys. We tested our approximation method on a one-dimensional model, where our CPA re-

sult is found to be in good agreement with "exact" result obtained by the Monte Carlo method. In particular, the disorder-induced asymmetrical broadening of the confined-state spectrum is well predicted by the CPA. We have also computed the conduction-band density of states $Al_xGa_{1-x}As$ superlattices using both the VCA and our method. Our approximate CPA spectra in the confined-state region are found to be down-shifted from the VCA spectra. The CPA spectra are also broadened, and exhibit intervalley scattering. Finally, we should point out that the technique developed here is not restricted in its application to superlattices; rather, it can be used to treat heterostructures of arbitrary profile.

ACKNOWLEDGMENTS

This work was supported by the University of Illinois Materials Research Laboratory under National Science Foundation Materials Research Laboratory (NSF-MRL) Grant No. DMR-83-16981, and the U.S. Office of Naval Research (ONR) under Contract No. N00014-81-K-0430.

[1]P. Soven, Phys. Rev. **156**, 809 (1967).

[2]B. Velický, S. Kirkpatrick, and H. Ehrenreich, Phys. Rev. **175**, 747 (1968).

[3]For a review of the subject, see H. Ehrenreich and L. M. Schwartz, in *Solid State Physics,* edited by H. Ehrenreich *et al.* (Academic, New York, 1976), Vol. 31, pp. 150–286.

[4]D. Stroud and H. Ehrenreich, Phys. Rev. B **2**, 3197 (1970).

[5]A. B. Chen and A. Sher, Phys. Rev. B **17**, 4726 (1978); **23**, 5360 (1981).

[6]K. C. Hass, H. Ehrenreich, and B. Velický, Phys. Rev. B **27**, 1088 (1983).

[7]D. Z.-Y. Ting and Y.-C. Chang, Phys. Rev. B **30**, 3309 (1984).

[8]Note: In the past, the CPA has been generalized to treat compositionally modulated alloys in A. Gonis and N. K. Flevaris, Phys. Rev. B **25**, 7544 (1982). Although the technique could be directly applied to treat superlattices, the amount of computation required is quite formidable for superlattices other than those with very short periods.

[9]A. B. Chen, Phys. Rev. B **7**, 2230 (1973).

[10]P. Dean, Proc. Phys. Soc. London **73**, 413 (1959); Proc. R. Soc. London, Ser. A **254**, 507 (1960); **260**, 263 (1961).

[11]D. N. Payton III and W. M. Visscher, Phys. Rev. **154**, 802 (1967).

[12]J. D. Dow, S. Y. Ren, and K. Hess, Phys. Rev. B **25**, 6218 (1982).

[13]W. A. Harrison, Phys. Rev. B **8**, 4487 (1973).

[14]J. C. Mikkelsen and J. B. Boyce, Phys. Rev. Lett. **49**, 1412 (1982); Phys. Rev. B **28**, 7130 (1983).

[15]A. Zunger and J. E. Jaffe, Phys. Rev. Lett. **51**, 662 (1983).

[16]K. C. Hass, R. J. Lempert, and H. Ehrenreich, Phys. Rev. Lett. **52**, 77 (1984).

[17]D. Z.-Y. Ting and Y.-C. Chang, Phys. Rev. B **36**, 4359 (1987); D. Z.-Y. Ting and Y.-C. Chang (unpublished).

[18]U. Venkateswaran, M. Chandrasekhar, H. R. Chandrasekhar, B. A. Vojak, F. A. Chambers, and J. M. Meese, Phys. Rev. B **33**, 8416 (1986).

[19]D. J. Wolford, T. F. Keuch, J. A. Bradley, M. A. Gell, D. Ninno, and M. Jaros, J. Vac. Sci. Technol. B **4**, 1043 (1986).

[20]J. Menéndez, A. Pinczuk, A. C. Gossard, J. H. English, D. J. Werder, and M. G. Lamont, J. Vac. Sci. Technol. B **4**, 1041 (1986).